

# Fractal and Multifractal Analysis of the Rise of Oxygen in Earth's Early Atmosphere

Satish Kumar

Manfred Cuntz

Zdzislaw E. Musielak

*Department of Physics, University of Texas at Arlington*

*Arlington, TX 76019;*

satish.kumar@mavs.uta.edu; cuntz@uta.edu; zmusielak@uta.edu

## ABSTRACT

The rise of oxygen in Earth's atmosphere that occurred 2.4 to 2.2 billion years ago is known as the Earth's Great Oxidation, and its impact on the development of life on Earth has been profound. Thereafter, the increase in Earth's oxygen level persisted, though at a more gradual pace. The proposed underlying mathematical models for these processes are based on physical parameters whose values are currently not well-established owing to uncertainties in geological and biological data. In this paper, a previously developed model of Earth's atmosphere is modified by adding different strengths of noise to account for the parameters' uncertainties. The effects of the noise on the time variations of oxygen, carbon and methane for the early Earth are investigated by using fractal and multifractal analysis. We show that the time variations following the Great Oxidation cannot properly be described by a single fractal dimension because they exhibit multifractal characteristics. The obtained results demonstrate that the time series as obtained exhibit multifractality caused by long-range time correlations.

*Subject headings:* Earth's Great Oxidation, Hurst exponent, fractal dimension, multifractal analysis.

## 1. INTRODUCTION

Fractal methods are well-suited for describing self-similarity, jaggedness and correlation of data sets. Typically, the data is characterized by the so-called fractal dimension, which can be evaluated by finding how the data fills its embedding space [1]. The data can be plotted and then the jaggedness of such graph can be compared to a straight line, leading to the box counting method or correlation integral methods. Another way is to treat the data as discrete and to compare it to uncorrelated noise, like in the well-known Hurst exponent method [2]. The fractal methods are generalized by multifractal methods that have different scaling moments for different moments or for different magnitudes of fluctuations. However, if a scaling component depends on the scale, there is a crossover, and the multifractal analysis must be separately applied to ranges of small and large scales. Typically, a singularity spectrum [3,4] is computed to determine multifractal characteristics of time series data.

The fractal and multifractal methods have been extensively applied to different problems in natural sciences, engineering, medicine, and the social sciences [3,4,5,6,7,8,9,10]. However, these methods have only been sparsely applied within the recently established field of astrobiology or its terrestrial counterpart, i.e., biogeology / geobiology, though the study by [11] on exoplanetary life detectability represents a notable exception. In this paper, we pursue another applications, a topic of great importance, namely, the rise of oxygen in Earth’s early atmosphere. It consists of the Earth’s Great Oxidation, followed by a more gradual increase of Earth’s atmospheric oxygen level.

In the following, we describe the problem in detail, and also explain why we chose the fractal and multifractal methods for this study. The Earth’s Great Oxidation occurred 2.4 to 2.2 billion years ago and it had a significant impact on Earth’s atmospheric physics and chemistry and, furthermore, entailed profound implications for the evolution of life. During this time span, the atmospheric oxygen concentration rose from less than  $10^{-5}$  of the present atmospheric level (PAL) to more than 0.01 PAL and possibly above 0.1 PAL [12,13,14,15]. Thereafter, a more gradual increase of the oxygen level occurred, eventually leading to today’s level. The rise of oxygen is still a topic of lively discussion owing to its wide ramifications regarding terrestrial and planetary astrobiology; specifically, it is still unclear whether Earth’s Great Oxidation occurred relatively smoothly or exhibited big jumps, i.e., akin to a yoyo model<sup>1</sup> (see [18]). Moreover, the entire sequence of oxygen increases, including

---

<sup>1</sup>Yoyo atmosphere is a term introduced by Ohmoto et al. (2006) [16] to refer to hypothetical oxygen in Earth’s atmosphere prior to the Great Oxidation. However, in the following this term is used as done by Cuntz et al. (2009) [17] to describe possible significant ups and downs of early Earth’s atmospheric oxygen amounts, which could also have occurred during or after the Great Oxidation.

the increase during the Proterozoic eon after the Great Oxidation, could have occurred relatively smoothly or by exhibiting intricate mathematical structures, which if present can only be uncovered through multifractal analysis.

Information on the rise of oxygen, especially the Great Oxidation, is in part based on studies of atmospheric sulphur chemistry, including analyses of multiple sulphur isotopes, as, e.g., the isotopic ratios between  $\Delta^{32}\text{S}$ ,  $\Delta^{34}\text{S}$ , and  $\Delta^{36}\text{S}$ ; see work by Farquhar et al. (2000) [19], Ohmoto et al. (2006) [16], Farquhar et al. (2007) [20], and Johnston (2011) [21] (in analogy using isotopic ratios to estimate the age of the Earth [22]). These studies indicate the patterns of increase of early Earth’s oxygen levels during different time intervals, including possible fluctuations. Studies providing additional insight into the long-standing debate regarding  $\text{O}_2$  in Earth’s early atmosphere include the work by Claire et al. (2006) [23], Lyons (2007) [24], Kaufman et al. (2007) [25], Kump (2008) [26], Balk et al. (2009) [27], Frei et al. (2009) [28], Freund et al. (2010) [29], Freund (2011) [30], and Flannery & Walter (2012) [31].

A set of nonlinear equations describing the time evolution of oxygen, methane and carbon in the early Earth was originally proposed and solved by Goldblatt et al. (2006) [32], thereafter GLW06, who encountered bistability in the system equations, which in their model represent the ancient Earth’s low-oxygen state ( $\lesssim 10^{-5}$  PAL) and the high-oxygen state ( $5 \times 10^{-3}$  PAL). Subsequent work by Cuntz et al. (2009) [17], thereafter CRM09, on the nonlinear set of equations further explored this system by replacing the original step function (GLW09) representing the reductant input rate by more realistic functions (i.e., exponential decay function, logistic decay function) with and without Gaussian white noise. Based on the transition stability analysis for the system equations, CRM09 considered a set of non-autonomous, nonlinear differential equations and furthermore inspected the Lyapunov exponents [33,34,35]. CRM09 found that the equations do not show chaotic behavior and that the rise of oxygen during the Great Oxidation occurred relatively smoothly.

Previous models of Earth’s Great Oxidation and the subsequent oxygen increase during the early Proterozoic eon have been based on a set of physical parameters that were determined using the available geological data as summarized by GLW06 and CRM09. However, it is well-known that this set of parameters is not unique because of potentially large uncertainties in the data. Therefore, it is the aim of the present work to expand those previous studies by adopting other sets of parameters and also analyzing the obtained results by using fractal and multifractal techniques. Specifically, we will use the standard Hurst exponent [2] and the fractal dimension related to it [1], as well as the Multifractal Detrended Fluctuation Analysis (MF DFA) [34], which was originally developed for non-stationary time series and required the so-called generalized Hurst exponents for computing a width of singularity spec-

trum (WSS). Our choice of using the MF DFA is motivated by the fact that our numerical solutions constitute non-stationary time series.

Our studies are performed for different strengths of white Gaussian noise, which is added to the system to account for possible variations in the physical parameters as well as for uncertainties in the adopted values of the parameters. We consider different levels of noise in the system and investigate their effects on the rise of oxygen as well as on the associated time variations of atmospheric methane and carbon in the Earth’s surficial environment. The effects of the noise are studied by performing fractal and multifractal analyses of our numerical results. We will be able to demonstrate that no single fractal dimension can be used to describe time variations of oxygen, carbon and methane because they exhibit multifractal characteristics due to long-range correlations of the small and large fluctuations in the time series.

Our paper is structured as follows: In §2, we describe the system equations considered in our study, the numerical method of solution, and the methods for performing the fractal and multifractal analysis. In §3, we present our results and discussion. Our conclusions are given in §4.

## 2. FORMULATION AND ANALYSIS TECHNIQUES

### 2.1. Original Governing Equations

The set of equations was originally given by GLW06 and was subsequently revisited by CRM09. It encompasses a simplified model of Earth’s global redox system, representing the atmosphere, ocean, and crust. Concerning the atmosphere and ocean, the number of moles of methane  $\mathcal{M}$  ( $\text{CH}_4$ ) and oxygen  $\mathcal{O}$  ( $\text{O}_2$ ) are calculated. Furthermore, with respect to the ocean floor, the amount of buried organic carbon  $\mathcal{C}$  in the crust is also computed. This leads to the following system of equations:

$$\frac{d\mathcal{M}}{dt} = \frac{1}{2}\Omega_{(\text{O}_2)}(N + r) - \frac{1}{2}\Psi_{(\text{O}_2)}\mathcal{M}^{0.7} - s\mathcal{M} - \frac{1}{2}\Omega_{(\text{O}_2)}\left[\beta(N + r) - w\mathcal{C}\right], \quad (1)$$

$$\frac{d\mathcal{O}}{dt} = \Omega_{(\text{O}_2)}N - (1 - \Omega_{(\text{O}_2)})r - \Psi_{(\text{O}_2)}\mathcal{M}^{0.7} - s\mathcal{M} - (1 - \Omega_{(\text{O}_2)})\left[\beta(N + r) - w\mathcal{C}\right], \quad (2)$$

and

$$\frac{d\mathcal{C}}{dt} = \beta(N + r) - w\mathcal{C}. \quad (3)$$

This set of differential equations is coupled and nonlinear because of the term  $\mathcal{M}^{0.7}$  as well as the functions  $\Omega_{(\text{O}_2)}$  and  $\Psi_{(\text{O}_2)}$ . Note that  $\Omega_{(\text{O}_2)}$  is given as  $\Omega_{(\text{O}_2)} = (1 - \gamma)(1 - \delta)$  with  $\gamma = \mathcal{O}/(d_\gamma + \mathcal{O})$  and  $\delta = \mathcal{O}/(d_\delta + \mathcal{O})$ , whereas  $\Psi_{(\text{O}_2)}$  is given as  $\Psi_{(\text{O}_2)} = 10^\epsilon$  with  $\epsilon = a_1\varphi^4 + a_2\varphi^3 + a_3\varphi^2 + a_4\varphi + a_5$ ,  $\varphi = \log \mathcal{O}$ ,  $a_1 = 0.0030$ ,  $a_2 = -0.1655$ ,  $a_3 = 3.2305$ ,  $a_4 = -25.8343$  and  $a_5 = 71.5398$ .

The different terms, parameters, and variables of Eqs. (1) to (3) require further detailed explanations. The first term on the RHS of  $d\mathcal{M}/dt$  and the corresponding terms of  $d\mathcal{O}/dt$  denote the net primary productivity for oxygenic photosynthesis  $N$  and the net input of reductant to the surface  $r$ , an electron donor for anoxygenic photosynthesis, which both depend on the time-variable oxygen concentration  $\mathcal{O}$ . Both GLW06 and CRM09 took  $N = 3.75 \times 10^{15}$  mol  $\text{O}_2$   $\text{yr}^{-1}$ . However, for  $r = r(t)$ , for which GLW06 chose a step function, exhibiting a downward jump from  $3 \times 10^{11}$  to  $7.5 \times 10^{10}$  mol  $\text{O}_2$  equiv.  $\text{yr}^{-1}$  at 2.4 Gyr, CRM09 adopted different functions, including functions incorporating statistical noise. This allowed them to consider the impact of different plausible reductant functions on early Earth’s atmospheric chemistry.

The work by GLW06 and CRM09 considered the dominant processes of the marine biosphere related to oxygenic photosynthesis and represented by an assumed net primary productivity of  $N$  mol  $\text{O}_2$   $\text{yr}^{-1}$ , implying that the total organic carbon produced is given as  $(N + r)$ . The fraction of this amount consumed by heterotrophic respirers is  $\gamma = \mathcal{O}/(d_\gamma + \mathcal{O})$  with  $d_\gamma = 1.36 \times 10^{19}$  mol. The fraction of the methane produced that is consumed by methanotrops is given as  $\delta = \mathcal{O}/(d_\delta + \mathcal{O})$ , where  $d_\delta = 2.73 \times 10^{17}$  mol. Therefore, the fraction of the oxygen and methane produced that reaches the atmosphere is given by  $\Omega_{(\text{O}_2)} = (1 - \gamma)(1 - \delta)$ . The next two terms on the RHS of Eqs. (1) and (2) correspond to the atmospheric methane oxidation reaction. Its rate can be obtained by fitting the results of detailed photochemical models, including the introduction of  $\Psi_{(\text{O}_2)}$ , which constitutes a polynomial function with respect to the amount of oxygen.

Once there is sufficient oxygen, Earth’s ozone layer forms, thus providing an effective shield against UV radiation. There are other terms in Eqs. (1) and (2) related to sinks and sources of atmospheric methane  $\mathcal{M}$ . Methane can be nullified by oxidation, but it can also be lost through hydrogen escape since methane is considered to be the sole source of hydrogen in the upper atmosphere with  $s = 3.7 \times 10^{-5}$   $\text{yr}^{-1}$  (GLW06) as a limiting flux constant. Detailed studies on the loss of hydrogen have been given by Hunten (1982) [37], Catling et al. (2001) [13], Zahnle et al. (2013) [38], among others. The final terms on the RHS of Eqs. (1) to (3) are due to the amount of buried organic carbon, which depends on the fraction  $\beta$ , taken as  $2 \times 10^{-3}$ , of the total organic carbon  $(N + r)$  that is produced. The rate of organic carbon weathering is  $w\mathcal{C}$ , where the bulk weathering rate  $w$ , given as  $w = 6 \times 10^{-9}$   $\text{yr}^{-1}$ ,

is set by analogy to present conditions and  $\mathcal{C}$  is the crustal organic carbon; see GLW06 and CRM09 for further details.

GLW06 obtained steady state solutions for methane and carbon given as  $\mathcal{M} = r/s$  and  $\mathcal{C} = \beta(N+r)/w$ , respectively. In case of oxygen, the steady state solution required obtaining the roots of a more complicated equation. In GLW06’s model, the solutions for oxygen, methane and carbon, exhibit bistability. This result, as previously pointed out by Kasting (2006) [18], arguably offers crucial insights into the bistable nature of Earth’s atmosphere, especially pertaining to the Great Oxidation, considering that the latter constitutes a switch to the high-oxygen (more than  $5 \times 10^{-3}$  PAL) steady state from a previous low-oxygen (less than  $10^{-5}$  PAL) steady state that existed for at least 300 million years even after the onset of oxygenic photosynthesis.

## 2.2. Modified Governing Equations with Noise

The main objective of our work is to add white Gaussian noise to the governing equations, i.e., Eqs. (1) to (3), in order to investigate its effect on the rise of oxygen in the early Earth’s atmosphere. We therefore introduce the following three new variables:  $\eta_{\mathcal{M}} = \sigma\kappa\mathcal{M}$ ,  $\eta_{\mathcal{O}} = \sigma\kappa\mathcal{O}$ , and  $\eta_{\mathcal{C}} = \sigma\kappa\mathcal{C}$ , where  $\sigma$  varies from 0.005 to 0.010, and  $\kappa$  is a random number given by a normal distribution with a mean of 0 and a variance of 1. Furthermore,  $\mathcal{M}$ ,  $\mathcal{C}$ , and  $\mathcal{O}$  represent the amounts of methane, carbon, and oxygen, respectively, as before. With the new variables added, Eqs. (1) to (3) read as

$$\frac{d\mathcal{M}}{dt} = \frac{1}{2}\Omega_{(\text{O}_2)}(N+r) - \frac{1}{2}\Psi_{(\text{O}_2)}\mathcal{M}^{0.7} - s\mathcal{M} - \frac{1}{2}\Omega_{(\text{O}_2)}[\beta(N+r) - w\mathcal{C}] + \eta_{\mathcal{M}} , \quad (4)$$

$$\frac{d\mathcal{O}}{dt} = \Omega_{(\text{O}_2)}N - (1 - \Omega_{(\text{O}_2)})r - \Psi_{(\text{O}_2)}\mathcal{M}^{0.7} - s\mathcal{M} - (1 - \Omega_{(\text{O}_2)})[\beta(N+r) - w\mathcal{C}] + \eta_{\mathcal{O}} , \quad (5)$$

and

$$\frac{d\mathcal{C}}{dt} = \beta(N+r) - w\mathcal{C} + \eta_{\mathcal{C}} . \quad (6)$$

These equations are solved using the geological and Earth’s atmospheric data as discussed by GLW06 and CRM09 (see §2.1). However, the new variables  $\eta_{\mathcal{M}}$ ,  $\eta_{\mathcal{O}}$ , and  $\eta_{\mathcal{C}}$  allow us to consider appropriate levels of noise for the terms  $d\mathcal{M}/dt$ ,  $d\mathcal{O}/dt$ , and  $d\mathcal{C}/dt$ , respectively, in the view of inherent uncertainties in the underlying geological processes.

Equations (4) to (6) are solved for different values of the noise strength  $\sigma$  by using the Euler-Maruyama method, which is suitable for the considered set of equations; additionally,

the resulting numerical errors are small. The obtained numerical results are displayed in 3D phase space defined by the variables  $\mathcal{O}$ ,  $\mathcal{C}$  and  $\mathcal{M}$ . We refer to such displays of our results as phase portraits whose main advantage is that they are able to show relationships between the three variables, and, furthermore, allow to demonstrate how the relationships change when the noise strength  $\sigma$  is varied. In order to determine how effectively the change occurs, we use the standard Hurst exponent [2] and the fractal dimension related to this exponent [1] as well as the so-called multifractal technique, which in §2.3.2 will be described in detail.

### 2.3. Analysis Techniques

#### 2.3.1. Hurst Exponent and Fractal Dimension

The standard Hurst exponent  $h$  was originally introduced by Hurst (1951) [2], who demonstrated that data described by  $h$  is anti-correlated if  $0 \leq h < 0.5$ , uncorrelated if  $h = 0.5$ , and correlated if  $0.5 < h \leq 1.0$ . According to Mandelbrot (1982) [1],  $h$  can be used to introduce the fractal dimension  $D_h = \epsilon - h$ , where  $\epsilon$  is the embedding space, and  $D_h$  is given as

$$D_h = \frac{1}{1-h} \quad 0 \leq h < 0.5 \quad (\text{anti-persistent}) \quad (7a)$$

$$D_h = 2.0 \quad h = 0.5 \quad (\text{non-persistent}) \quad (7b)$$

$$D_h = \frac{1}{h} \quad 0.5 < h \leq 1.0 \quad (\text{persistent}) . \quad (7c)$$

The above definition of  $D_h$  is known to provide a smooth transition from anti-persistent to persistent including the point  $h = 0.5$ , and to be robust for measuring macro-trends in the data [4].

#### 2.3.2. Multifractal Technique

We analyze the results of our numerical simulations by using the Multifractal Detrended Fluctuation Analysis (MFDFA), which is used to compute the so-called generalized Hurst exponents  $h(q)$  and a width of singularity spectrum; note that the generalized Hurst exponents  $h(q)$  becomes the standard Hurst exponent  $h$  if  $q = 2$ . Let us now briefly describe the MFDFA method by following the notation and steps originally introduced by Kantelhardt et al. (2002) [36]. We begin by calculating the profile for a given series  $Y(i)$ , where

$i = 1, 2, \dots, N$ , using

$$Y(i) = \sum_{k=1}^i [x_k - \langle x \rangle], \quad (8)$$

profile into  $N_s = N/s$  non-overlapping segments of equal length  $s$ . In general,  $N$  may not be a multiple of  $s$ , thus in order to account for a small part remaining at the end of the series, we repeat the same procedure but this time by starting from the end of the series; note that reverting the series does not affect the multifractal behavior of the series as all its parameters remain the same. Since the procedure is used twice,  $2N_s$  segments are obtained.

We determine a possible local trend of the series by the least-square polynomial fit of the series. Thereafter, we calculate the variance by using

$$F^2(\nu, s) = \frac{1}{s} \sum_{i=1}^s [Y((\nu - 1)s + i) - y_\nu(i)]^2 \quad (9a)$$

for the segments  $\nu = 1, 2, \dots, N_s$ , and

$$F^2(\nu, s) = \frac{1}{s} \sum_{i=1}^s [Y(N - (\nu - N_s)s + i) - y_\nu(i)]^2 \quad (9b)$$

for the segments  $\nu = N_s + 1, \dots, 2N_s$ , with  $y_\nu(i)$  being the fitting polynomial in segment  $\nu$ .

With the variance known, we compute the moment dependent fluctuation function

$$F_q(s) = \left[ \frac{1}{2N_s} \sum_{\nu=1}^{2N_s} [F^2(\nu, s)]^{q/2} \right]^{1/q}. \quad (10a)$$

Note that for  $q = 2$ , the above analysis becomes the detrended fluctuation analysis (DFA). However, for other values of  $q$ , the multifractal behavior is characterized by different Hurst exponents at different scales, the so-called generalized Hurst exponent, which requires the computation of the fluctuating function at different moments.

The power law behavior is displayed in log–log plots of the fluctuating function  $F_q(s) \sim s^{h(q)}$ , where the generalized Hurst exponent  $h(q)$  converges to the standard Hurst exponent  $h$  of the series. Since scales  $s < 10$  and  $s > N/4$  lead to systematic statistical errors, we take the values between them. Moreover,  $F_q(s)$  diverges for  $q = 0$ , which means that it cannot be calculated using Eq. (9a, 9b); therefore, we compute it by using a logarithmic average given as

$$F_q(s) = \exp \left[ \frac{1}{4N_s} \sum_{\nu=1}^{2N_s} \ln [F^2(\nu, s)] \right] \sim s^{h(0)}. \quad (10b)$$



The generalized Hurst exponent is related to the classical scaling exponent  $\tau(q)$  through the following relation  $\tau(q) = qh(q) - 1$ .

There is also another way of characterizing the multifractal series. It involves introducing the so-called singularity spectrum  $f(\xi)$ , which is related to  $\tau(q)$  via a Legendre transform, i.e.,  $\xi = \tau'(q)$  and  $f(\xi) = q\xi - \tau(q)$ , with  $\xi$  being the singularity strength or Hölder exponent; note that the WSS provides a measure of strength of multifractal behavior, and that it is used in this study to analyze the results of our numerical simulations.

### 3. RESULTS AND DISCUSSION

#### 3.1. Numerical Results

We solve Eqs. (4) through (6) by using the Euler-Maruyama method. The input parameter  $r(t)$ , i.e., the net input of reductant to the surface, is specified as given by the exponential function  $r(t) = r_0 \exp(-\alpha t/t_0)$ , with  $r_0 = 3.5 \times 10^{11}$  mol O<sub>2</sub> equiv. yr<sup>-1</sup>,  $\alpha = 1.4$ , and  $t_0 = 1.0 \times 10^7$  yr. In addition, we assume that the initial number of oxygen molecules is  $10^8$  mol and use a step size of  $10^{-3}$  yr. Our numerical computations indicate time-dependent changes for the amounts of oxygen, methane and carbon. The changes of oxygen in time are presented in Fig. 1, which shows an initially smooth, but steep rise within the first  $10^3$  years, and then oscillatory behavior, which is driven by the noise. It is this oscillatory behavior, which mostly occurs after the Great Oxidation, i.e., during the early Proterozoic eon, we wish to focus on. Our study will be pursued in the 3D phase space defined by the variables describing carbon, oxygen and methane of the system.

The obtained phase portraits for different strengths of noise are shown in Figs. 2 and 3; note that our numerical results obtained for the first  $10^3$  years have been omitted. The phase portraits show the relationships between the carbon, oxygen and methane variables as well as the extent of the 3D phase space covered by these relationships for the different levels of noise. By inspecting the phase portraits, we find that different strengths of noise correspond to remarkably different depictions in the phase space. However, there is not a clear correlation between the strength of noise and the volume of the 3D phase space covered by the relationships. Therefore, as the next step we perform the fractal and multifractal analysis of our numerical results.

Through this analysis, we want to determine whether the resulting numerical time series describing variations of carbon, oxygen and methane in our model of the early Earth is a fractal system that requires a single exponent or fractal dimension, or a multifractal system that is characterized by a continuous spectrum of exponents or the WSS. The analysis will

also allow us to identify the nature of multifractality, i.e., whether it is due to probability distributions or long-range correlations.

### 3.2. Generalized Hurst exponent and fractal dimension

We compute the generalized Hurst exponent  $h$  by using the MFDFA and taking  $q = 2$ , which means that the resulting  $h$  is equivalent to the standard Hurst exponent [2]. The values of  $h$  obtained for different strengths of the noise introduced to the system are shown in the second column of Table 1. It is seen that  $h$  is not sensitive to the different values of noise strengths and that it is close to 0.5, which implies that the numerically computed time series data is uncorrelated.

Having obtained  $h$ , we use the results presented in §2.3 to calculate the fractal dimension  $D_h$ . The computed values of  $D_h$  are given in the third column of Table 1. It is seen that  $D_h$  is largely independent of the strength of the noise, which is an expected result because of the  $D_h$  dependence on  $h$ . This obviously implies that our numerically computed time series of variations of carbon, oxygen and methane in our model of the early Earth cannot be fully characterized by one single exponent or fractal dimension. Therefore, our main conclusions about the effects of noise on our numerical results must arise from the multifractal analysis and the concept of the WSS.

### 3.3. Multifractal analysis

Following §2.3, we perform a multifractal analysis based on the MFDFA, which was used to compute the WSS, where the WSS represents the distance between two end points of the singularity spectrum, i.e., the first and last values of the Hölder exponent  $\xi$ . Note that the higher the value of the WSS, the stronger is the multifractal characteristics of the time series. The computed values of the WSS are given in the last column of Table 1.

It is found that the value of the WSS is clearly the highest for the strength of noise  $\sigma = 0.005$  and the lowest for  $\sigma = 0.010$ . There is an obvious trend indicating a negative slope between these values in terms of a  $\sigma$ -WSS relationship, albeit the existence of scatter, which is most evident regarding  $\sigma = 0.008$ , where the value for the WSS is close to the minimum value at  $\sigma = 0.010$ . In order to gauge the significance of the decline of the WSS values as function of  $\sigma$ , we applied a two-tailed Spearman  $r$  correlation analysis (e.g., [39]). The Spearman  $r$  is identified as  $-0.71$  with a standard deviation of 0.11, hence confirming the suspected functional decline. Thus, the general trend of the decreasing WSS with increasing

values of  $\sigma$  appears to be valid for our numerically generated time series.

The observed trend is an indication that white Gaussian noise changes the multifractal characteristics of our time series, which is contrary to the fractal dimension that is about the same for all time series as shown in the third column of Table 1. Therefore, the inclusion of the noise makes a significant contribution to the overall behavior of oxygen and methane in our model of Earth’s early atmosphere and to carbon present in early Earth’s surficial environment. Additionally, our results show that this contribution can only be determined by using the multifractal analysis, which is in agreement with the earlier finding [40,41] that a true signal is distinguished from superimposed noise if MFDFA is employed in natural time [42].

The above analysis was performed for the white Gaussian noise with  $\sigma$  varying from 0.005 to 0.010. Since it is difficult to reliably account for uncertainties in historic geological data, let us extend our analysis through considering so-called ‘pink noise’, while assuming that  $\sigma$  varies from 0.005 to 0.009. Our results are given in Table 2. Our calculations show again that the fractal dimension is not sensitive to the different values of the noise and, moreover, that the WWS exhibits a small, but still notable increasing trend with decreasing strength of noise  $\sigma$ . To further explore this dependency, we consider pink noise with  $\sigma_{\mathcal{C}}$ ,  $\sigma_{\mathcal{M}}$ , and  $\sigma_{\mathcal{O}}$ , corresponding to the variables  $\mathcal{C}$ ,  $\mathcal{M}$ , and  $\mathcal{O}$ , respectively. Furthermore, we assume that  $\sigma_{\mathcal{O}}$  varies from 0.005 to 0.009, and that  $\sigma_{\mathcal{C}} = \sigma_{\mathcal{M}} = 0.005$ . The obtained results are given in Table 3, which shows that the trend of WWS is similar to that attained in the last column of Table 2.

Having established the multifractal characteristics of the time series, the series has then been randomized and the WSS has been used to identify the nature of its multifractality. In general, multifractality can be either due to a broad probability density function for the values of the time series, or due to different long-range time correlations of the small and large fluctuations in the time series, or both. The obtained results show that our time series exhibit multifractality caused by long-range time correlations of the small and large fluctuations in the time series. This is an important result, as it shows that the numerically generated time series of oxygen, carbon and methane still have some statistical correlations even if they are separated by very long time intervals.

## 4. CONCLUSIONS

In this study we expand on previous work aimed at modeling the rise of oxygen in Earth’s atmosphere encompassing both the Great Oxidation and early stages of the gradual

oxygen increase during the Proterozoic eon. Experimentally, information on this process has been obtained through extended biogeological studies. This field of research is obviously of significant importance for historical terrestrial studies, but it has also potentially profound implications for the growing fields of exobiology and planetary science.

In a previous paper, GLW06 presented a mathematical model for the time-dependent behavior of carbon, methane and oxygen based on a set of nonlinear differential equations. This model incorporated numerous geological, atmospheric, biological and biochemical processes, and was able to reproduce the bifurcated nature of Earth’s ancient atmosphere consisting of a low-oxygen (less than  $10^{-5}$  PAL) and a high-oxygen state (more than  $5 \times 10^{-3}$  PAL), including the transition between the two. This model was subsequently extended by CRM09 who studied details of the switch between the two stages using more general step functions for the underlying biogeological process. The aim of this work was to explore whether or not the switch occurred in jumps (yoyo-model) or exhibited a more gradual oxygen concentration increase.

In the present work we further augmented this model by investigating the effects of the noise on the time variations of oxygen, carbon and methane by using fractal and multifractal analysis techniques. The overall goal was to offer a more realistic picture by accounting for uncertainties in the geological data, which led us to add different strengths of noise within the original equations describing Earth’s ancient atmosphere. Our results confirm the relatively smooth oxygen increase previously described by CRM09; however, we also consider the behavior of Earth’s atmospheric oxygen level in the time span following the Great Oxidation, i.e., the early Proterozoic eon. For that time span, the obtained results show that the numerically generated time series describing the time variations of oxygen, carbon and methane cannot properly be described by a single fractal dimension because they exhibit multifractal characteristics. We also demonstrated that our time series exhibit the multifractality caused by the long-range time correlations of the small and large fluctuations in the time series. We regard this work as a further step toward elucidating the complex biogeochemical processes of the early Earth, which gave rise to the previously identified oxygen increase, among other dynamic developments. Additional studies may also require to consider more complex geodynamic and geobiological models for the early Earth, which are currently developed by other research groups.

We would like to thank the two reviewers for their valuable comments that allowed us to significantly improve our original manuscript. This work has been supported in part by the SETI Institute (M. C.) as well as by the Alexander von Humboldt Foundation (Z. E. M.) and by the University of Texas at Arlington through its Faculty Development Program (Z. E. M.).

## REFERENCES

- [1] Mandelbrot BB. The fractal geometry of nature. San Francisco: Freeman; 1982.
- [2] Hurst HE. Long-term storage capacity of reservoirs. *Trans Amer Soc Civ Eng* 1951;116:770–808.
- [3] Falconer K. Fractal geometry. Mathematical foundations and applications. New York: John Wiley & Sons; 1990.
- [4] Gouyet J-F. Physics and fractal structures. New York: Springer; 1996.
- [5] Peitgen H-O, Jürgens H, Saupe D. Chaos and fractals. New York: Springer; 2003.
- [6] Wu X, Wang J, Lu J, Iu HHC. Hyperchaotic behavior in a non-autonomous unified chaotic system with continuous periodic switch. *Chaos, Solitons & Fractals* 2007;32:1485–90.
- [7] Lopes R, Betrouni N. Fractal and multifractal analysis: a review. *Medical Image Analysis* 2009;13:634–49.
- [8] Varotsos PA, Sarlis NV, Skordas ES, Lazaridou, MS. Fluctuations, under time reversal, of the natural time and the entropy distinguish similar looking electric signals of different dynamics. *J Appl Phys* 2008;103:014906(12pp.).
- [9] Varotsos PA, Sarlis NV, Skordas ES. Detrended fluctuation analysis of the magnetic and electric field variations that precede rupture. *Chaos* 2009;19:023114(7pp.).
- [10] Sarlis NV, Skordas ES, Varotsos PA. Nonextensivity and natural time: The case of seismicity. *Phys Rev E* 2010;82:021110(79pp.).
- [11] Azua-Bustos A, Vega-Martínez C. The potential for detecting ‘life as we don’t know it’ by fractal complexity analysis. *Int J Astrobiol* 2013;12:314–20.
- [12] Brocks JJ, Logan GA, Buick R, Summons RE. Archean molecular fossils and the early rise of eukaryotes. *Science* 1999;285:1033–36.
- [13] Catling DC, Zahnle KJ, McKay CP. Biogenic methane, hydrogen escape, and the irreversible oxidation of early earth. *Science* 2001;293:839–43.
- [14] Kasting JF. The rise of atmospheric oxygen. *Science* 2001;293:819–20.
- [15] Kasting JF, Siefert JL. Life and the evolution of earth’s atmosphere. *Science* 2002;296:1066–8.

- [16] Ohmoto H, Watanabe Y, Ikemi H, Poulson SR, Taylor BE. Sulphur isotope evidence for an oxic archaean atmosphere. *Nature* 2006;442:908–11.
- [17] Cuntz M, Roy D, Musielak ZE. The great oxidation of earth’s atmosphere: contesting the yoyo model via transition stability analysis. *Astrophys J Lett* 2009;706:L178–L82 [CRM09].
- [18] Kasting JF. Ups and downs of ancient oxygen. *Nature* 2006;443:643–5.
- [19] Farquhar J, Bao H, Thiemens M. Atmospheric influence of earths earliest sulfur cycle. *Science* 2000;289:757–59.
- [20] Farquhar J, Peters M, Johnston DT, Strauss H, Masterson A, Wiechert U et al. Isotopic evidence for mesoarchaean anoxia and changing atmospheric sulphur chemistry. *Nature* 2007;449:706–9.
- [21] Johnston DT. Multiple sulfur isotopes and the evolution of earth’s surface sulfur cycle. *Earth-Science Rev* 2011;106:161–83.
- [22] Varotsos PA. Calculation of point defect parameters in diamond. *Phys Rev E* 2007;75:172107(3pp.); Erratum 2008;78:059902(1p.).
- [23] Claire MW, Catling DC, Zahnle KJ. Biogeochemical modelling of the rise in atmospheric oxygen. *Geobiology* 2006;4:239–69.
- [24] Lyons TW. Palaeoclimate: oxygen’s rise reduced. *Nature* 2007;448:1005–6.
- [25] Kaufman AJ, Johnston DT, Farquhar J, Masterson AL, Lyons TW, Bates S et al. Late archaean biospheric oxygenation and atmospheric evolution. *Science* 2007;317:1900–3.
- [26] Kump LR. The rise of atmospheric oxygen. *Nature* 2008;451:277–8.
- [27] Balk M, Bose M, Ertem G, Rogoff DA, Rothschild LJ, Freund FT. [2009] Oxidation of water to hydrogen peroxide at the rockwater interface due to stress-activated electric currents in rocks earth. *Planet Sci Lett* 2009;283:87–92.
- [28] Frei R, Gaucher C, Poulton SW, Canfield DE. Fluctuations in precambrian atmospheric oxygenation recorded by chromium isotopes. *Nature* 2009;461:250–3.
- [29] Freund FT, Balk M, Rothschild LJ. Is there nothing else to oxidize the early earth but oxygenic photosynthesis? *Astrobiology Science Conference 2010: Evolution and life: surviving catastrophes and extremes on earth and beyond. LPI Contribution* 2010;1538:5640.

- [30] Freund FT. Pre-earthquake signals: underlying physical processes. *J Asian Earth Sci* 2011;41:383–400.
- [31] Flannery DT, Walter MR. Archean tufted microbial mats and the great oxidation event: new insights into an ancient problem. *Austral J Earth Sci* 2012;59:1–11.
- [32] Goldblatt C, Lenton TM, Watson AJ. Bistability of atmospheric oxygen and the great oxidation. *Nature* 2006;443:683–6 [GLW06].
- [33] Baker GL, Gollub JP. *Chaotic dynamics: An introduction*. Cambridge, UK: Cambridge Univ Press; 1990.
- [34] Hilborn RC. *Chaos and nonlinear dynamics*. Oxford: Oxford Univ. Press; 1994.
- [35] Musielak ZE, Musielak DE. High-dimensional chaos in dissipative and driven dynamical systems. *Int J Bifurcation and Chaos* 2009;19:2823–69.
- [36] Kantelhardt JW, Zschiegner SA, Koscielny-Bunde E, Havlin S, Bunde A, Stanley HE. Multifractal detrended fluctuation analysis of nonstationary time series. *Physica A* 2002;316:87–114.
- [37] Hunten DM. Thermal and nonthermal escape mechanisms for terrestrial bodies. *Planet Space Sci* 1982;30:773–83.
- [38] Zahnle K, Catling DC, Claire MW. The rise of oxygen and the hydrogen hourglass. *Chem Geology* 2013;362:26–34.
- [39] Press WH, Flannery BP, Teukolsky SA, Vetterling WT. *Numerical recipes*. Cambridge, UK: Cambridge Univ Press; 1986.
- [40] Varotsos PA, Sarlis NV, Skordas ES. Long-range correlations in the electric signals that precede rupture: Further investigations. *Phys Rev E* 2003;67:021109(13pp.); Erratum 2008;78:059902(1p.).
- [41] Varotsos PA, Sarlis NV, Skordas ES. Attempt to distinguish electric signals of a dichotomous nature. *Phys Rev E* 2003;68:031106(7pp.).
- [42] Varotsos PA, Sarlis NV, Skordas ES. Long-range correlations in the electric signals that precede rupture. *Phys Rev E* 2002;66:011902(7pp.); Erratum 2008;78:059902(1p.).

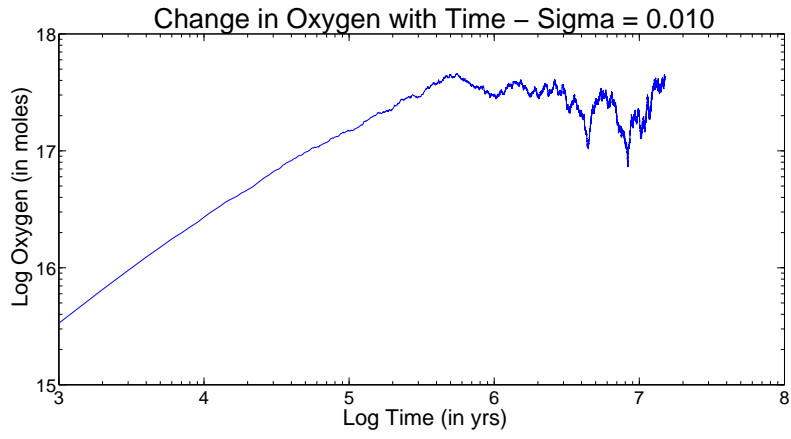
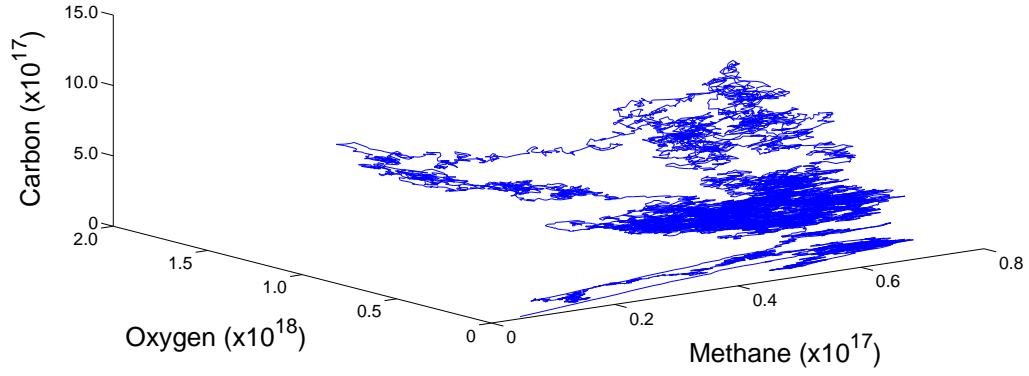


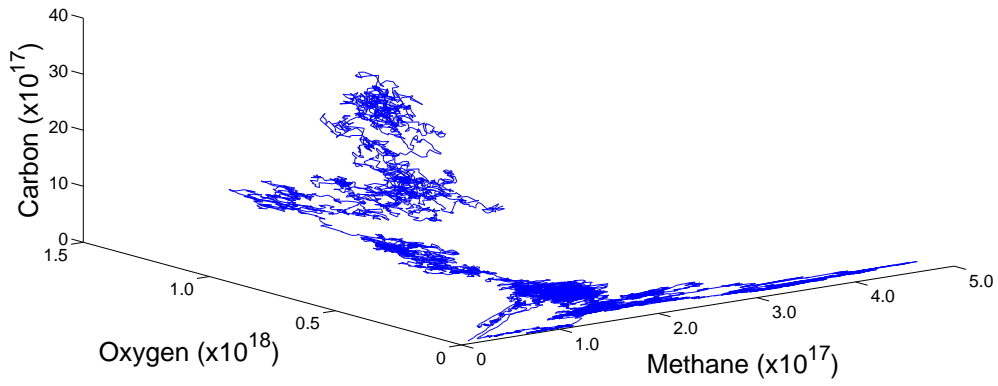
Fig. 1.— Variations of oxygen with time in the early Earth’s atmosphere for a noise strength of  $\sigma = 0.010$ . Note that  $3 \times 10^{17}$  mol of  $O_2$  corresponds to 0.01 PAL.



Noise Strength 0.005



Noise Strength 0.006



Noise Strength 0.007

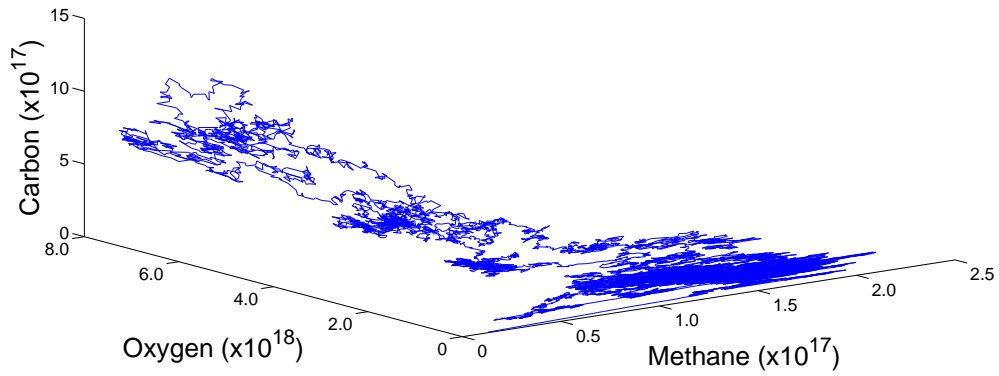
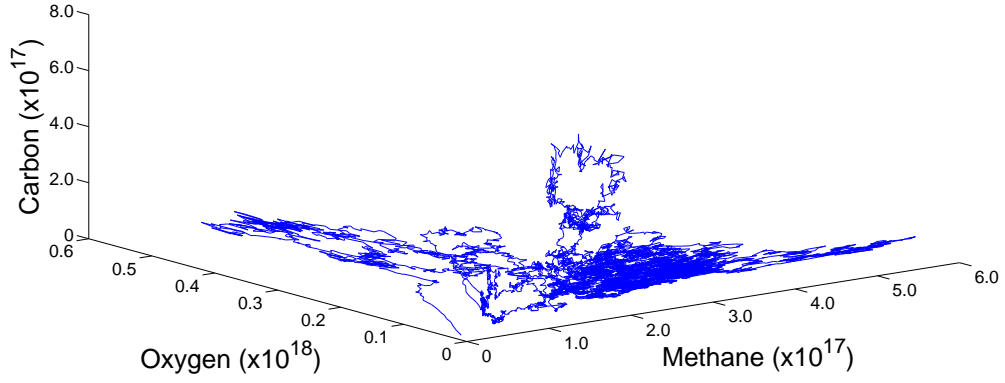
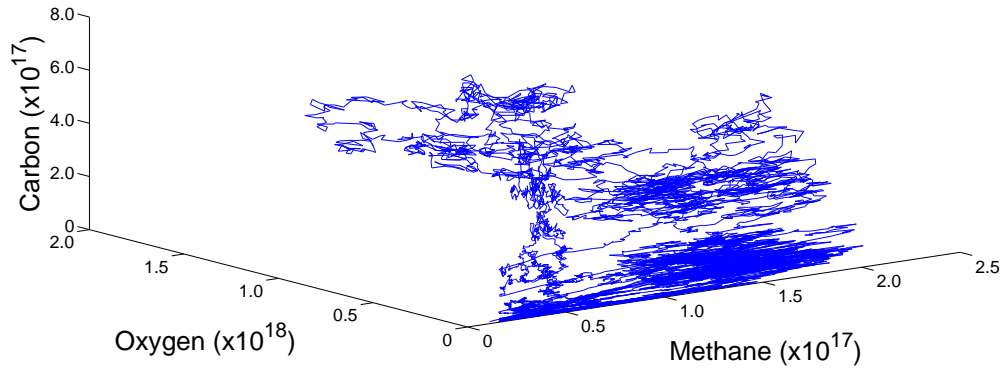


Fig. 2.— Phase portraits of our numerical results obtained for noise strengths of  $\sigma = 0.005$ , 0.006, and 0.007. Note the differences in the various scales.

Noise Strength 0.008



Noise Strength 0.009



Noise Strength 0.010

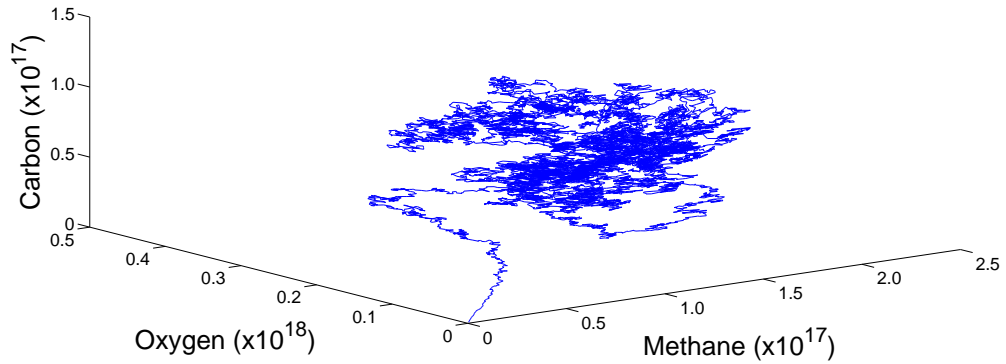


Fig. 3.— Phase portraits of our numerical results obtained for noise strengths of  $\sigma = 0.008$ , 0.009, and 0.010. Note the differences in the various scales.

Table 1. Fractal and multifractal analysis of numerical results with white Gaussian noise

Noise strength $\sigma$	Generalized Hurst exponent $h$ at $q = 2$	Fractal dimension $D_h$	WSS
0.005	0.5087	3.4913	1.2080
0.006	0.5104	3.4896	1.0760
0.007	0.5032	3.4968	1.1609
0.008	0.5457	3.4543	0.8647
0.009	0.5325	3.4675	1.0918
0.010	0.5206	3.4794	0.8110

Table 2. Fractal and multifractal analysis of numerical results with pink noise

Noise strength $\sigma$	Generalized Hurst exponent $h$ at $q = 2$	Fractal dimension $D_h$	WSS
0.005	0.4496	3.5504	0.8196
0.006	0.4310	3.5690	0.8191
0.007	0.4486	3.5514	0.9876
0.008	0.4467	3.5533	0.8045
0.009	0.4361	3.5639	1.0165

Table 3. Fractal and multifractal analysis of numerical results with pink noise and  $\sigma_{\mathcal{O}}$  varying from 0.005 to 0.009, and  $\sigma_{\mathcal{L}} = \sigma_{\mathcal{M}} = 0.005$ .

Noise strength $\sigma$	Generalized Hurst exponent $h$ at $q = 2$	Fractal dimension $D_h$	WSS
0.005	0.4496	3.5504	0.8196
0.006	0.4692	3.5308	0.6779
0.007	0.4786	3.5214	0.8045
0.008	0.4578	3.5422	0.7622
0.009	0.4582	3.5418	0.9527